

PDE-Based Bayesian Hierarchical Modeling for Event Spread, with Application to COVID-19 Infection

Mengqi Cen¹, Xuejing Meng², X. Joan Hu³, Juxin Liu⁴, and Jianhong Wu⁵

¹Department of Population Medicine, Harvard Pilgrim Health Care Institute, Boston, Massachusetts, USA, mengqi_cen@hphci.harvard.edu

²School of Statistics and Mathematics and Collaborative Innovation Center of China Pilot Reform Exploration and Assessment Hubei Sub-Center, Hubei University of Economics, Wuhan, China., mengxuejing18@163.com

³Corresponding author, Department of Statistics and Actuarial Science, Simon Fraser University, Burnaby, Canada., joanh@stat.sfu.ca

⁴Department of Mathematics and Statistics, University of Saskatchewan, Saskatoon, Canada., jul086@mail.usask.ca

⁵Department of Mathematics and Statistics, York University, Toronto, Canada., wujh@mathstat.yorku.ca

Abstract

We extended the Wikle’s Bayesian hierarchical model based on a diffusion-reaction equation [Wikle, 2003] to investigate the COVID-19 spatio-temporal spread events across the USA from Mar 2020 to Feb 2022. Our model incorporated an advection term to account for the intra-state spread trend. We applied a Markov chain Monte Carlo (MCMC) method to obtain samples from the posterior distribution of the parameters. We implemented the approach via the collection of the COVID-19 infections across the states overtime from the New York Times. Our analysis shows that our approach can be robust to model misspecification to a certain extent and outperforms a few other approaches in the simulation settings. Our analysis results confirm that the diffusion rate is heterogeneous across the USA, and both the growth rate and the advection velocity are time-varying.

1 Introduction

Coronavirus disease (COVID-19) emerged in December 2019, and has rapidly spread into a pandemic of the world since then. Millions of confirmed cases have been reported globally. The United States, for example, has more than 80 million infected people as of Mar 31, 2022 [The New York Times, 2022].

In response to the ongoing pandemic, numerous studies have been conducted to understand and predict the spread of COVID-19. The most commonly used models are the compartmental models. The population is assigned to compartments according to the infectious status, and the transfer rates between compartments are estimated. For instance, the susceptible-infectious-recovered (SIR) model with time-varying transmission rates is used to predict the epidemic trend of COVID-19 [Jia et al., 2020]. Cooper et al. predict the spread of the virus using the extended SIR model with time-varying total and susceptible population [Cooper et al., 2020]. Other models, such as the Susceptible-Infected-Recovered-Deceased (SIRD), Susceptible-Exposed-Infectious-Removed (SEIR) and Susceptible-Exposed-Infectious-Quarantined-Removed (SEIQR) models, are developed by including more compartments [Bousquet et al., 2022, Delli Compagni et al., 2022, Sun et al., 2020]. These models are based on ordinary differential equations (ODEs), and are only applicable to studying disease processes over time. Given that most regions do not follow complete isolation, modeling the spread in both space and time is desirable and can be more realistic.

To investigate event spatio-temporal spread, the diffusion process is widely used [Wikle, 2003, Brauer et al., 2019]. Consider the general advection-diffusion partial differential equation (PDE):

$$\frac{\partial}{\partial t}u(t; s) = \nabla \cdot \delta(s)\nabla u(t; s) + \zeta u(t; s), \quad (1)$$

where $u(t; s)$ is the spatio-temporal process of interest with $s = (x, y)^T \in \mathcal{S}$ at time $t \in \mathcal{T}$, $\delta(s)$ is the spatially varying diffusion coefficient and ζ is a growth coefficient. Here $\nabla = (\frac{\partial}{\partial x}, \frac{\partial}{\partial y})^T$ is the gradient operator, and for a vector field $F = (F^x, F^y)$, $\nabla \cdot F = \frac{\partial F^x}{\partial x} + \frac{\partial F^y}{\partial y}$ is the divergence operator. This PDE has been applied to model the spread of COVID-19: δ represents the speed of spread between neighbouring regions, and ζ indicates the speed of spread within a region [Wang and Yamamoto, 2020, Yamamoto et al., 2021].

Motivated by patterns shown in the American COVID-19 data from the New York Times [The New York Times, 2022], we consider an advection-diffusion-reaction PDE in this paper. The extended PDE is widely used in many areas especially in environment and ecology [Hundsdoerfer and Verwer, 2007, Sigris et al., 2015].

When analytic solutions are absent, the finite difference method (FDM) is frequently used to approximate the solution of a PDE [Smith et al., 1985]. It solves differential equations by replacing the derivatives with their finite difference approximations. First-order forward differences in time and centred differences in space are extensively used to approximate spatio-temporal processes; see, for example Lu et al. [2020] and Williams et al. [2019]. This paper uses FDM to approximate the solution of the advection-diffusion-reaction PDE, which defines the latent spatio-temporal process underlying the event spread.

This paper is structured as follows. Section 2 starts with a descriptive analysis of the American COVID-19 data. Section 3 elaborates the PDE-based Bayesian hierarchical model and presents the computational techniques using MCMC methods for parameter estimation. In Section 4, the proposed approach is assessed by simulation studies. It is followed by COVID-19 data analysis. Section 5 includes conclusions and comments regarding future investigations.

2 American COVID-19 Data from Jan 21, 2020 to Mar 31, 2022

We downloaded the records of American COVID-19 infections from *the New York Times* on April 1, 2022. The data were gathered from the local health agencies' reports, including the number of daily cumulative lab-confirmed cases in each American county from Jan 21, 2020, to Mar 31, 2022.

Figure 1 shows the confirmed case numbers of the mainland USA during the selected periods. Each point is located at the centre of a county, and the size of the point is proportional to the county's case counts. The plot suggests that the spread does not have the same diffusion rate in all directions. Thus, the PDE in (1) is not sufficient to explain the spread of the virus. An advection term should be included to explain the tendency of the virus for movement in a specific direction.

Figure 1 in the Supplementary Materials presents the daily cases with a 7-day moving average in the USA. There were three large spikes in the confirmed case numbers over the past two years. The trend of case counts is clearly varying over time. It suggests that a more generalized model with time-varying parameters should be considered.

3 Hierarchical Bayesian Analysis

3.1 PDE-Based Bayesian Hierarchical Modeling

We introduce a hierarchical Bayesian model to explore the event spatio-temporal spread on a regular grid. The hierarchical Bayesian modeling consists of three stages: the first stage specifies the distribution of the data, the second stage formulates a latent process, and the last stage assigns the prior distribution to the parameters in the model.

3.1.1 Modeling Event Counts

Let $n(t; s)$ be the total number of events of interest in location $s = (x, y)^T \in \mathcal{S}$ at time $t \in \mathcal{T}$. Assume $n(t; s)$ follows a Poisson distribution with mean $\lambda(t; s)$:

$$n(t; s) \mid \lambda(t; s) \sim \text{Poisson}(\lambda(t; s)). \quad (2)$$

Here we assume that $n(t; s)$ and $n(t'; s')$ are independent conditional on their means $\lambda(t; s)$ and $\lambda(t'; s')$ for either $t \neq t'$ or $s \neq s'$.

3.1.2 Latent Process Specification

Since the Poisson intensity can take only positive real values, we consider $u(t; s) = \log(\lambda(t; s))$. To take other important factors into account, one may consider $u(t; s) = \log(\lambda(t; s)) - \log(c(t; s))$, where $c(t; s)$ is the population size at location s at time t in COVID-19 application. We specify $u(t; s)$, a latent spatio-temporal process, in the following.

To describe the latent spatio-temporal process underlying a collection of bird migration data, Wikle considers a diffusion-reaction equation with a space-varying diffusion rate as shown in (1). This partial differential equation (PDE) is widely used in modeling ecological and epidemic processes, for instance, the expansion of Eurasian Collared-Dove [Hooten and Wikle, 2008] and the indoor spread of coronavirus [Ahmed et al., 2021].

Motivated by the American COVID-19 data, we consider adding an advection term into the PDE in (1) to capture the spatio-temporal trend of the spread. The advection-diffusion-reaction PDE is:

$$\frac{\partial}{\partial t} u(t; s) = -\boldsymbol{\nu}(t; s) \nabla u(t; s) + \nabla \cdot \delta(s) \nabla u(t; s) + \zeta(t) u(t; s), \quad (3)$$

where $\boldsymbol{\nu}(t; s) = (\nu_1(t; s), \nu_2(t; s))$. Here $\nu_1(t; s)$ and $\nu_2(t; s)$ measure the tendency of the virus to move in the positive direction of the x- and y-axis. The drift velocity and growth rate can be time-independent with $\boldsymbol{\nu}(t; s) \equiv (\nu_1(s), \nu_2(s))$ and $\zeta(t) \equiv \zeta$ for all t .

Denote $u_t(x, y) = u(t; s)|_{s=(x, y)}$, we approximate $u(t; s)$ in (3) using the following equation:

$$\begin{aligned} \tilde{u}_t(x, y) = & u_{t-\Delta t}(x, y)[1 - 2\delta(x, y)(\frac{\Delta t}{\Delta^2 x} + \frac{\Delta t}{\Delta^2 y}) + \zeta_{t-\Delta t}\Delta t] \\ & + u_{t-\Delta t}(x - \Delta x, y)[\frac{\Delta t}{4\Delta^2 x}\{4\delta(x, y) - \delta(x + \Delta x, y) + \delta(x - \Delta x, y) + 2\nu_{1,t-\Delta t}(x, y)\Delta x\}] \\ & + u_{t-\Delta t}(x + \Delta x, y)[\frac{\Delta t}{4\Delta^2 x}\{4\delta(x, y) + \delta(x + \Delta x, y) - \delta(x - \Delta x, y) - 2\nu_{1,t-\Delta t}(x, y)\Delta x\}] \\ & + u_{t-\Delta t}(x, y + \Delta y)[\frac{\Delta t}{4\Delta^2 y}\{4\delta(x, y) + \delta(x, y + \Delta y) - \delta(x, y - \Delta y) - 2\nu_{2,t-\Delta t}(x, y)\Delta y\}] \\ & + u_{t-\Delta t}(x, y - \Delta y)[\frac{\Delta t}{4\Delta^2 y}\{4\delta(x, y) - \delta(x, y + \Delta y) + \delta(x, y - \Delta y) + 2\nu_{2,t-\Delta t}(x, y)\Delta y\}], \end{aligned} \quad (4)$$

where $s = (x, y)$ represents a rectangular region $[x - \frac{1}{2}\Delta x, x + \frac{1}{2}\Delta x] \times [y - \frac{1}{2}\Delta y, y + \frac{1}{2}\Delta y]$. It is an approximation of the solution of PDE by first-order forward differences in time and centred differences in space.

We express $u(t; s)$ in vector form based on (4):

$$\mathbf{u}(t; s) = \mathbf{H}(\boldsymbol{\delta}, \zeta(t - \Delta t), \boldsymbol{\nu}(t - \Delta t))\mathbf{u}(t - \Delta t) + \boldsymbol{\epsilon}(t; s), \quad (5)$$

where $\mathbf{H}(\boldsymbol{\delta}, \zeta(t - \Delta t), \boldsymbol{\nu}(t - \Delta t))$ is a n -dim vector, $\mathbf{u}(t - \Delta t)$ represents the vector with the spatio-temporal process at all the locations at the previous time point, and $\boldsymbol{\epsilon}(t; s)$ is the error term and we assume $\boldsymbol{\epsilon}(t; s) \sim N(0, \sigma^2)$ iid. Alternatively, we can consider errors with autoregressive structure:

$$\boldsymbol{\epsilon}(t; s) = \phi\boldsymbol{\epsilon}(t - \Delta t; s) + \boldsymbol{\eta}(t; s), \quad (6)$$

and assume $\phi \sim U(-1, 1)$, $\boldsymbol{\eta}(t; s) \sim N(0, \sigma^2)$.

In the COVID-19 application, we let $s \in \mathcal{S} = \{1, 2, \dots, 26\}$ as shown in Figure 2 A. We consider evenly-spaced time points $t \in \mathcal{T} = \{1, 2, \dots, 23\}$, where $t = 1$ and $t = 23$ respectively represents April 2020 and Feb 2022. We set $\Delta t = 1$ to be one month. Given that the spread over a long period is of interest, it is sufficient to use the monthly data. When more detailed temporal features are desired, smaller time units can be used at the cost of increased computation times.

3.1.3 Prior Distribution of Parameters

Assume for any t and s , the advection, diffusion and growth terms follow normal distribution:

$$\begin{aligned} \nu_1(t; s) &\sim N(\tilde{\nu}_1, \tilde{\sigma}_{\nu_1}^2), \quad \delta(s) \sim N(\tilde{\delta}, \tilde{\sigma}_{\delta}^2), \\ \nu_2(t; s) &\sim N(\tilde{\nu}_2, \tilde{\sigma}_{\nu_2}^2), \quad \zeta(t) \sim N(\tilde{\zeta}, \tilde{\sigma}_{\zeta}^2). \end{aligned} \quad (7)$$

In addition, we let $\delta(s) \geq 0$, and $\sigma^2 \sim IG(\tilde{q}, \tilde{r})$. The parameters with the “tilde” are hyperparameters that are previously specified. The choices for the hyperparameters can be based on the prior knowledge from the transmission of the infectious disease in other regions. In cases when this information is limited, we choose vague prior distributions.

3.2 Estimation Procedure

The following posterior distribution summarises the Bayesian formulation of the proposed hierarchical model:

$$\begin{aligned} & [\boldsymbol{\nu}_{1,0}, \dots, \boldsymbol{\nu}_{1,T-1}, \boldsymbol{\nu}_{2,0}, \dots, \boldsymbol{\nu}_{2,T-1}, \boldsymbol{\delta}, \zeta_0, \dots, \zeta_{T-1}, \sigma^2, \phi, \mathbf{u}_1, \dots, \mathbf{u}_T \mid \mathbf{n}_1, \dots, \mathbf{n}_T] \\ & \propto \left\{ \prod_{t=1}^T [\mathbf{n}_t \mid \mathbf{u}_t] \right\} \times \left\{ \prod_{t=1}^T [\mathbf{u}_t \mid \boldsymbol{\nu}_{1,t-1}, \boldsymbol{\nu}_{2,t-1}, \boldsymbol{\delta}, \zeta_{t-1}, \mathbf{u}_{t-1}, \sigma^2, \phi] \right\} \\ & \times [\boldsymbol{\nu}_{1,0}] \dots [\boldsymbol{\nu}_{1,T-1}] [\boldsymbol{\nu}_{2,0}] \dots [\boldsymbol{\nu}_{2,T-1}] [\boldsymbol{\delta}] [\zeta_0] \dots [\zeta_{T-1}] [\sigma^2] [\phi]. \end{aligned} \quad (8)$$

Since the posterior distribution is not analytically tractable, Markov chain Monte Carlo (MCMC) methods are applied to obtain samples from the posterior distribution of the parameters. The procedure was carried out using RStan [Stan Development Team, 2022] in R [R Core Team, 2021].

After the prior and the sampling distribution are specified, the Gibbs sampler cycles through the full conditional distribution for the parameters. After the Markov chains converge, each parameter's point estimate is obtained using its posterior mean.

4 Numerical Studies

4.1 Simulation Study

We conduct a simulation study to assess the proposed approaches numerically. In simulation settings, we set $T = 24$ and $S = 5 \times 5 = 25$ grids. The true values of parameters are provided in Table 1, and the hyperparameters used in both scenarios are provided in Table 2. In both the scenarios, the counts drift to the bottom-right corner for $t = 1, \dots, 12$ and drift in the opposite direction for $t = 13, \dots, 24$. Also, the growth rate is high initially and then drops to about 0.

4.1.1 Scenario 1: Time-varying Growth Rate, Space-varying Diffusion Rate, and Time- and Space-varying Advection Speed

We generated data based on the proposed model 3 and conducted analyses under the first four models as listed in Table 3. The data generating process is as follows:

```

for  $t \leftarrow 1$  to 24 do
  Calculate vector  $\mathbf{H}(\delta, \zeta(t-1), \nu(t-1))$  based on (4);
  for  $s \leftarrow 1$  to 25 do
    Generate the errors:  $\epsilon(t; s) \sim N(0, \sigma^2)$  iid;
    Calculate the spatio-temporal process  $u(t; s)$  following (5);
    Calculate the Poisson intensity process:  $\lambda(t; s) = \exp(u(t; s))$ ;
    Generate counts:  $n(t; s) \sim \text{Poisson}(\lambda(t; s))$ ;
  end
end

```

Algorithm 1: Data Generating Process in Scenario 1

We conducted the analyses of the generated data utilizing the four aforementioned models. By the MCMC method described in Section 3.2, samples were obtained from the posterior distribution for each parameter. 50,000 MCMC samples were drawn, with the first 20,000 as the burn-in. The values of R-hats, a diagnostic statistics comparing the variation between chains to the variation within the chains, are all close to 1. It verifies the adequacy of the burn-in period.

The true values and the posterior means of the parameters and $\mathbf{u}(t; s)$ are shown in Figure 2 and 3 in the Supplementary Materials. The mean squared errors (MSEs) associated with each model are also shown in Figure 3 in the Supplementary Materials. The proposed model 3 outperforms the other three models with the closest estimates of the parameters and the lowest MSE values.

4.1.2 Scenario 2: Process with Autoregressive Errors

In this scenario, we generate data from the proposed model 3 with autoregressive errors to examine the robustness of the estimation procedure. We kept the same true values for the parameters as in the first scenario.

The data generating process was the same as the steps in scenario 1 with exception in the generation of $\epsilon(t; s)$. We assume

$$\epsilon(t; s) = \phi \epsilon(t-1; s) + \eta(t; s), \quad (9)$$

where $\eta(t; s) \sim N(0, 0.1)$, and $\phi = 0.1$. These values were selected since they are close to the COVID-19 analysis results in the following section.

The true values and the estimation of parameters for all the models are shown in Figure 3. Figure 4 illustrates the true values and the estimated values of \mathbf{u}_t with all the models. The proposed model 3 again produces a reasonable estimation of parameters and \mathbf{u}_t , indicating its robustness to model misspecification.

We consider four different prior variances for advection, diffusion and reaction rates for proposed model 3. Figure 4 in Supplementary Materials shows the estimated parameters for different prior distributions. The estimates are close to the true values when the variance is less than or equal to 0.01. It indicates certain robustness of the analysis under the proposed model 3. However, estimates can differ from the true values when the prior variances are large, which motivates the proposed model 5, specifying correlations between the random errors.

4.2 Data Analysis: COVID-19 Infection

We apply the proposed approach to investigate the spread of the COVID-19 infection in the USA from Mar 2020 to Mar 2022 using the data file downloaded from *The New York Times*.

4.2.1 Monthly Confirmed Cases Aggregated by Grids

We divide the mainland USA into 26 equal-area grid cells, with each covering 174,807 miles square, as shown in Figure 2. The size of the cells depends on the selection of Δx and Δy in (4). Higher resolution grids can be used if more detailed spatial features are desired, at the expense of longer computation times. Figure 5 A presents log-transformed aggregated counts by the grid using the geographic coordinates for each county from US Census Bureau [US Census Bureau, 2021]. This plot again shows that the spatio-temporal process involves great variability over space and time. Figure 2 B illustrates how monthly cases vary in each grid cells, demonstrating that the counts have an uncertain tendency over time. Since population sizes vary across cells, the counts alone cannot accurately reflect the level of disease. Population-adjusted case maps and line plots are shown in Figure 5 B and Figure 2 C, respectively. This allows us to compare the level of disease in different populations.

4.2.2 Bayesian Analysis: Spread of COVID-19 with Hierarchical Bayesian Model

We consider six different models specified in Table 3 to investigate the spread of COVID-19 in the USA. In proposed model 5, we consider both autoregressive structure error and population-adjusted latent process. We account for the spatial variations in the control measures and other factors using space-varying diffusion rate and drift velocity. The growth rate is assumed space-independent based on the findings from Figure 5 B. This is because the potential major factors, such as the availability of vaccines and the emergence of variants, are similar across the country. In addition, we consider the drift velocity and growth rate to be time-varying since there is great variability of case counts over time according to the COVID-19 data, as shown in Figure 2 C. Given that most of the temporal spread is modelled by these two parameters, the additional time-varying feature of the diffusion rate is unnecessary.

Other models are nested in model 5. The monthly confirmed cases from Mar 2020 to Feb 2022 are used as input data. After obtaining the parameter estimates, we make predictions for case numbers in Mar 2022 and compare them to the real counts from *The New York Times*.

Table 4 gives the hyperparameter values used in all of our analyses. Given the limited information on the parameters, we choose vague priors by forcing the variances to be relatively large. It is verified that the analyses are not sensitive to the selections of the hyperparameters by testing with three different sets of prior values listed in Table 4.

We run three Markov chains for each parameter using RStan. 300,000 samples are drawn from the posterior distribution from each chain, with the first 150,000 considered burn-in. The R-hats are close to 1, indicates that the chains converged.

Figure 6 illustrates the estimate of the parameters with their posterior mean under each model. The growth rate in proposed model 2-5 fluctuate over time and follows a similar pattern as presented in Figure 1 in the Supplementary Materials. The spatial map of the posterior mean for the diffusion rate, δ , suggests significant heterogeneity in the diffusion of the latent process. Figure 6 also includes the estimated $\nu(t; s)$, the trend of spread, where the size of the arrow is proportional to the value of advection speed in each grid. The analysis results confirm that the advection velocity are time-varying. In proposed model 5, the 95% credible interval for ϕ is [0.231, 0.238] indicates that it is significantly different from 0.

We make predictions for case numbers in Mar 2022 following the steps below. Here, $t = 23$ and $t = 24$ represents Feb 2022 and Mar 2022, respectively.

```

for  $t = 23$  do
  | Obtain posterior mean for each of  $\phi$ ,  $\delta$ ,  $\epsilon(t)$ ,  $\zeta(t)$ ,  $\nu_1(t)$ ,  $\nu_2(t)$  and  $\mathbf{u}(t)$ ;
  | Calculate matrix  $\mathbf{H}(\delta, \zeta(t), \nu_1(t), \nu_2(t))$  based on (4);
end
for  $t = 24$  do
  | Estimate  $\mathbf{u}(t) = \mathbf{H}\mathbf{u}(t-1) + \phi\epsilon(t-1) + \log(\mathbf{p})$ , where  $\mathbf{p}$  is a vector of population;
end

```

Algorithm 2: Prediction Procedure for Case Numbers in Mar 2022

Figure 7 illustrates the difference between the log-transformed observed cases and the prediction of the log-transformed cases in Mar 2022. The proposed models with time-varying ζ outperform other models since they have closer estimations to the true values of parameters.

5 Discussion

This paper aims to develop a tool to explore the spatio-temporal spread of events. We attempt to understand the spread features of events and make predictions about the future. Our modeling is partly motivated by the American coronavirus infection data. We introduce an advection-diffusion-reaction PDE with space- and

time-varying parameters to a hierarchical Bayesian framework. Along with FDM and MCMC methods, we implement the procedure and estimate the parameters in the models. The proposed approach can be applied to analyze other types of spatio-temporal data, for example, the number of deaths or hospitalizations due to COVID-19 infection.

We consider an additional advection term and the time-varying feature of parameters based on the model proposed by Wikle. These modifications play important roles on understanding the spread of events as shown in the prediction of American COVID-19 confirmed cases in Mar 2022. The parameter estimates are far away from the true values if we consider original model.

There are a few worthwhile future investigations along the line of dependence of the key quantities on time, location and other exposures. This paper considers the growth rate and advection velocity as piecewise constant. As we mentioned in Section 2, the trend of case counts is largely affected by many factors, such as the control measures or the emergence of the variants of coronavirus. We could further modify the model by considering the key quantities as the functions of time, location, and other potential covariates.

The error term is assumed to be independent across space in the process modeling. However, this assumption might be too strong. The counts are likely correlated with each other spatially. Future investigations are still needed for understanding the impact of possible spatial dependence.

Other future investigations includes: evaluating the process given parameters rather than generating the process from the joint distribution of parameters and process; choosing smaller or dynamic partition for Δx , Δy and Δt based on the data; considering alternative boundary conditions [Wikle, 2003].

A Tables

Table 1: The True Values of Parameters Used in Both Simulation Scenarios

parameter	true value	parameter	true value
$\delta(s)$ for $s = 1, \dots, 25$	0.1	σ^2	0.1
$\zeta(t)$ for $t = 0, \dots, 5$	0.15	$\zeta(t)$ for $t = 6, \dots, 23$	0.01
$\nu_1(t)$ for $t = 0, \dots, 11$	0.1	$\nu_1(t)$ for $t = 12, \dots, 23$	-0.1
$\nu_2(t)$ for $t = 0, \dots, 11$	0.1	$\nu_2(t)$ for $t = 12, \dots, 23$	-0.1

Table 2: Hyperparameters Used in Both Simulation Scenarios

parameter	true value	parameter	true value
$\tilde{\nu}_1$	0	$\tilde{\nu}_2$	0
$\tilde{\sigma}_{\nu_1}^2$	0.1	$\tilde{\sigma}_{\nu_2}^2$	0.1
$\tilde{\delta}$	0	$\tilde{\zeta}$	0
$\tilde{\sigma}_{\delta}^2$	0.1	$\tilde{\sigma}_{\zeta}^2$	0.1
\tilde{q}	0.001	\tilde{r}	0.001

Table 3: Description of Models

Models	TV ζ	SV ζ	TV δ	SV δ	TV ν	SV ν	PA	AR ϵ
Wikle	\times	\times	\times	\checkmark	/	/	\times	\times
Proposed Model 1	\times	\times	\times	\checkmark	\times	\checkmark	\times	\times
Proposed Model 2	\checkmark	\times	\times	\checkmark	\times	\checkmark	\times	\times
Proposed Model 3	\checkmark	\times	\times	\checkmark	\checkmark	\checkmark	\times	\times
Proposed Model 4	\checkmark	\times	\times	\checkmark	\checkmark	\checkmark	\checkmark	\times
Proposed Model 5	\checkmark	\times	\times	\checkmark	\checkmark	\checkmark	\checkmark	\checkmark

Notes: TV, time-varying; SV, space-varying; PA, population-adjusted; AR, autoregressive.

Table 4: Values of the Hyperparameters

parameter	Set 1	Set 2	Set 3
$\tilde{\nu}_1$	0	0	0.1
$\tilde{\nu}_2$	0	0	0.1
$\tilde{\sigma}_{\nu_1}^2$	10	100	10
$\tilde{\sigma}_{\nu_2}^2$	10	100	10
$\tilde{\delta}$	0	0	0.1
$\tilde{\zeta}$	0	0	0.1
$\tilde{\sigma}_{\delta}^2$	10	100	10
$\tilde{\sigma}_{\zeta}^2$	10	100	10
\tilde{q}	0.001	0.001	0.001
\tilde{r}	0.001	0.001	0.001

B Figures

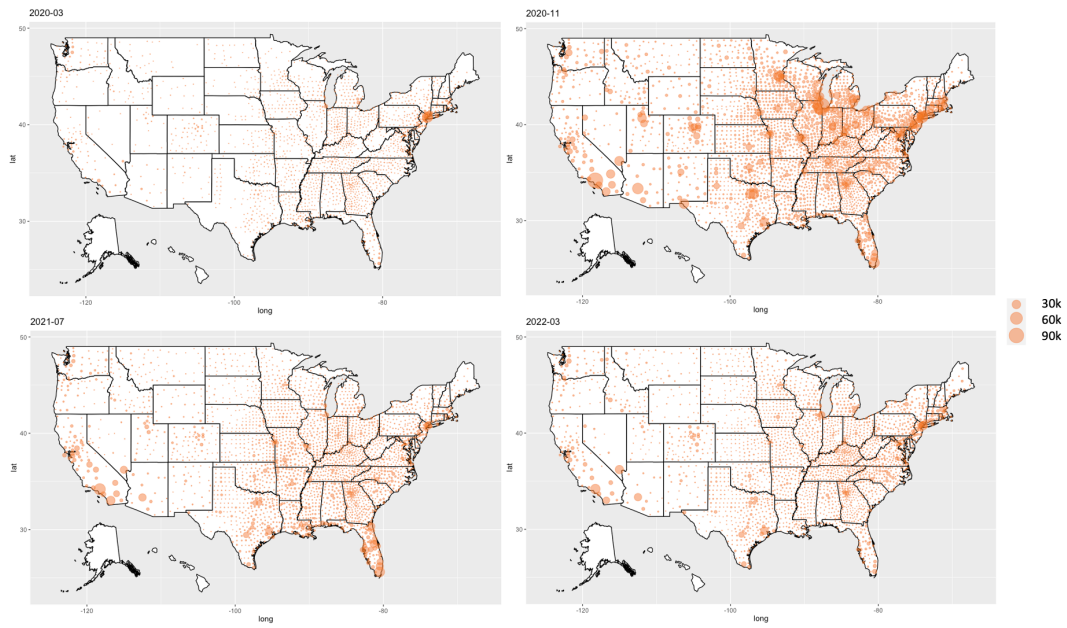


Figure 1: The Confirmed COVID-19 Cases in the USA for Selected Months

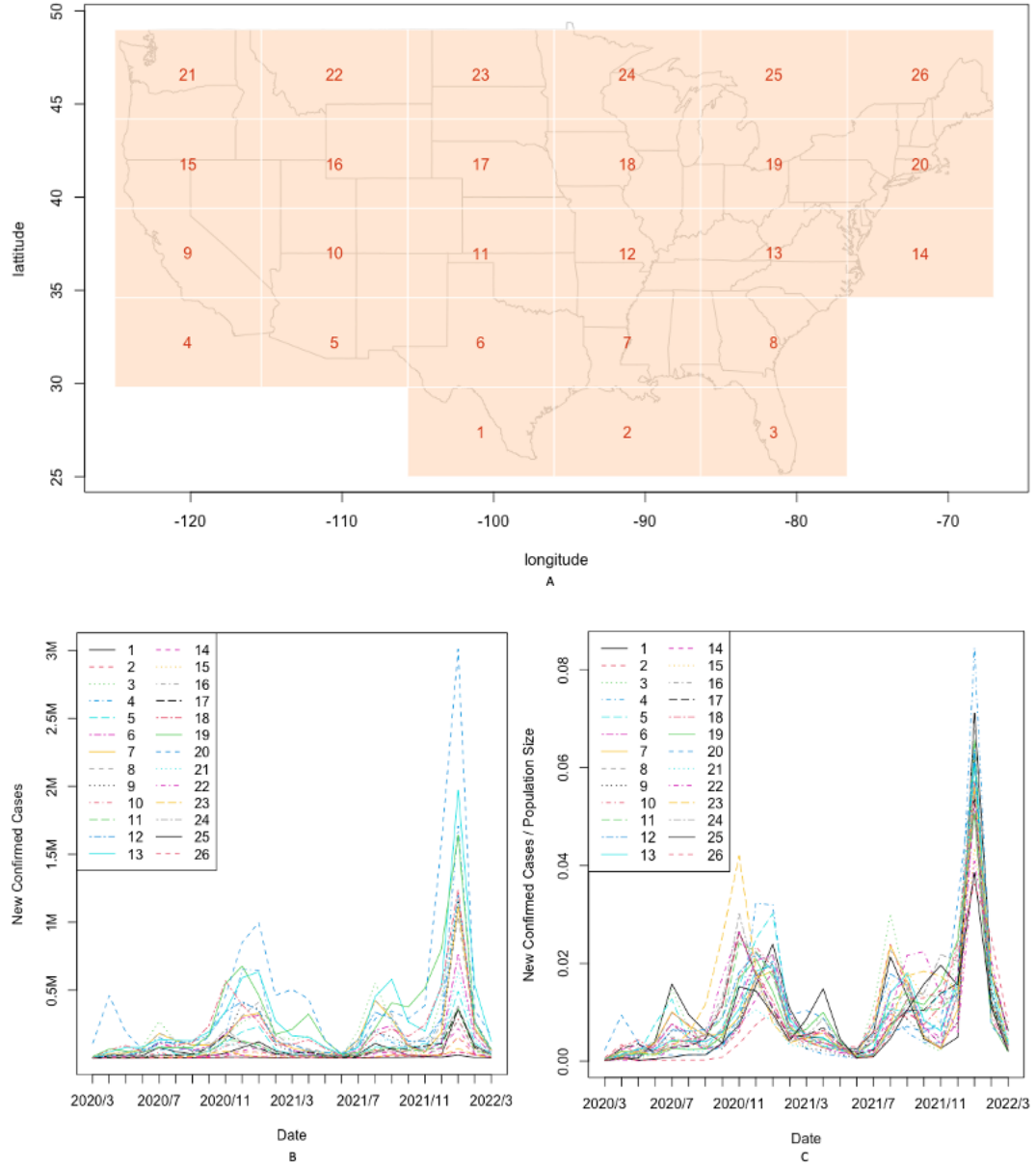


Figure 2: A. Grids with the Partition in the Example: Location $s = 1, \dots, S = 26$; B. Monthly Confirmed New Cases; and C. Monthly Confirmed New Cases divided by the Population Sizes across Different Locations

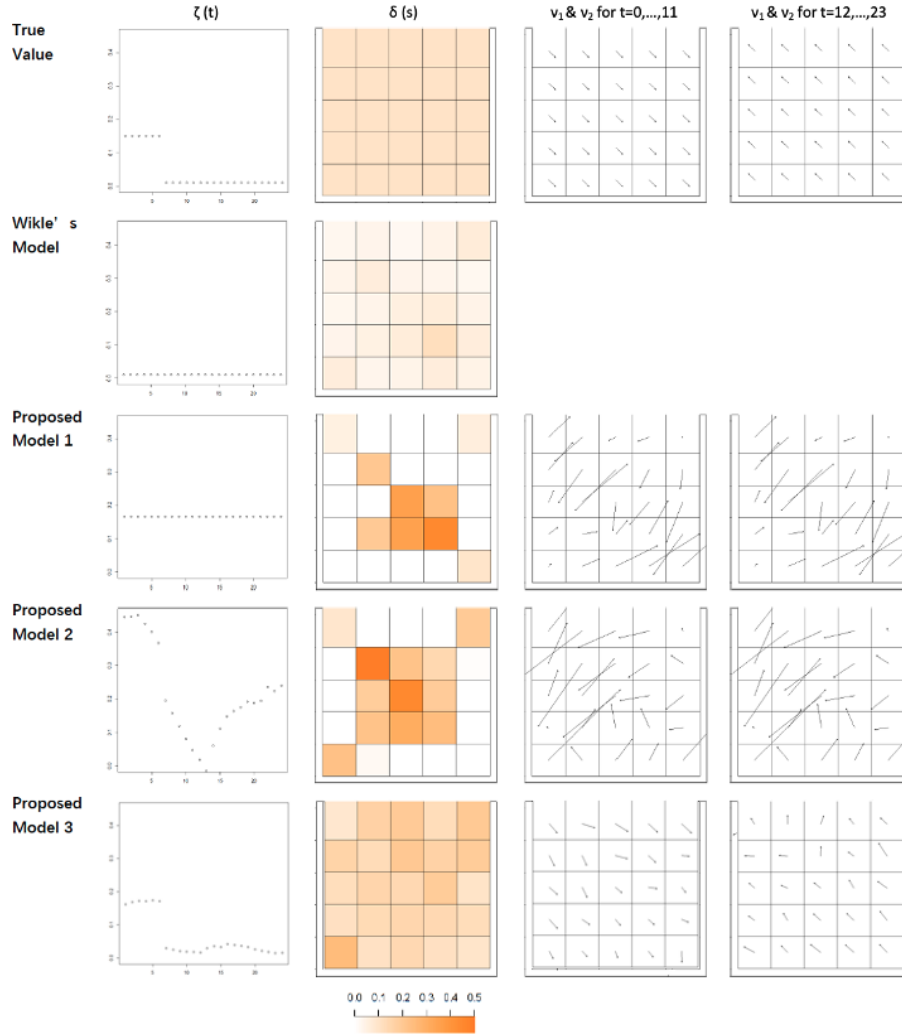


Figure 3: The True Values and the Posterior Means of Parameters with Different Models in Simulation Scenario 2

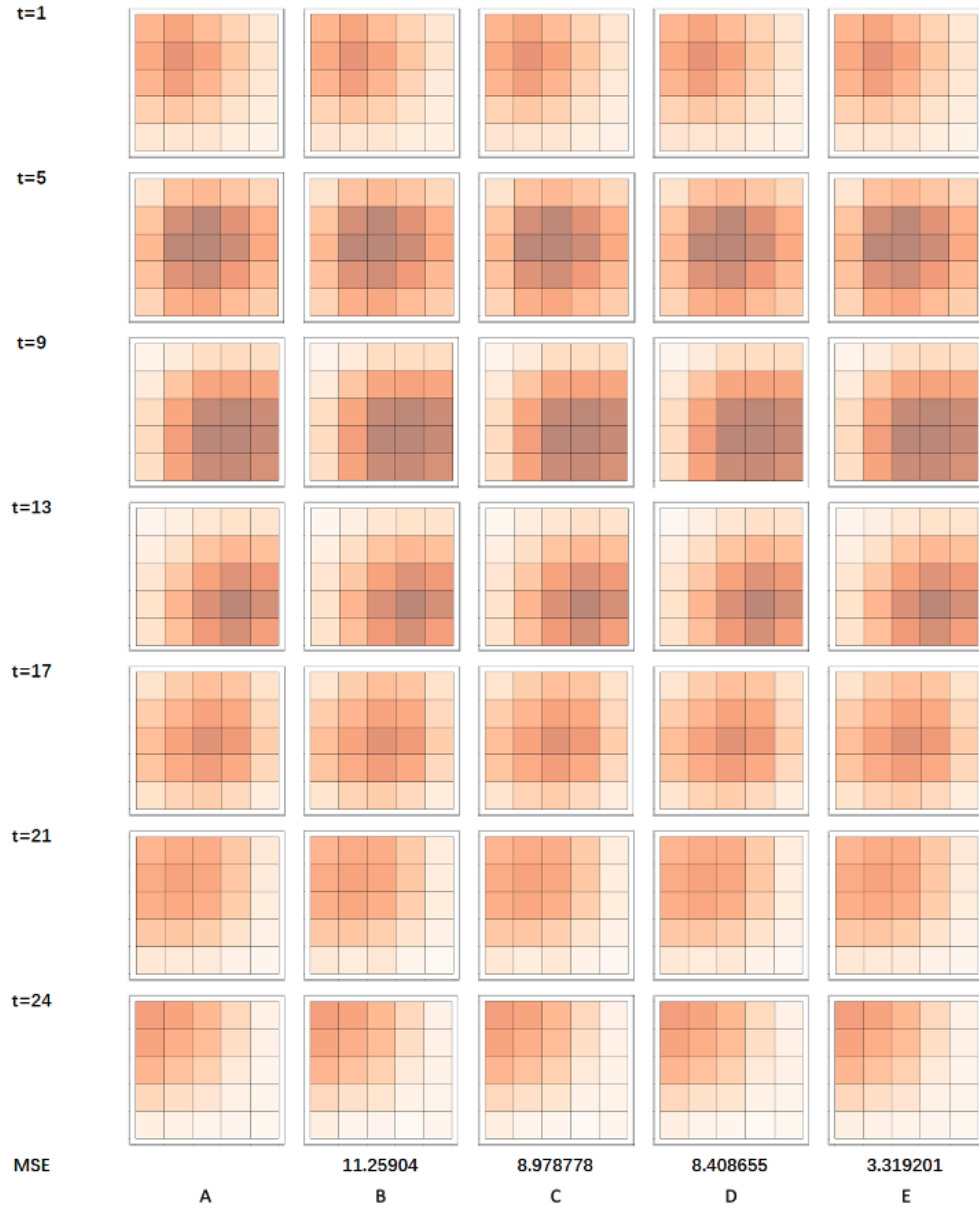


Figure 4: A. The True Values of \mathbf{u}_t ; the Estimated Values of \mathbf{u}_t with B. Wike's Model, C. Proposed Model 1, D. Proposed Model 2 and E. Proposed Model 3 in Simulation Scenario 2



Figure 5: A. Log-transformed Number of Confirmed Cases Aggregated by Grids; B. Population-Adjusted Log-transformed Number of Confirmed Cases Aggregated by Grids



Figure 6: Posterior Means of Parameters in Each Model

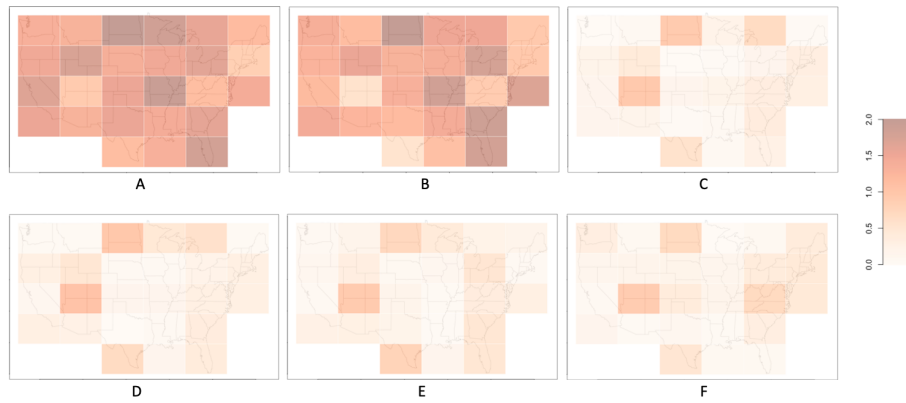


Figure 7: Difference between Log-transformed Observed Counts in Mar 2022 with Prediction of Log-transformed Counts under A. Wike's Model, B. Proposed Model 1, C. Proposed Model 2, D. Proposed Model 3, E. Proposed Model 4 and F. Proposed Model 5

References

- Nauman Ahmed, Amr Elsonbaty, Ali Raza, Muhammad Rafiq, and Waleed Adel. Numerical simulation and stability analysis of a novel reaction–diffusion covid-19 model. *Nonlinear Dynamics*, 106(2):1293–1310, 2021.
- Arthur Bousquet, William H Conrad, Said Omer Sadat, Nelli Vardanyan, and Youngjoon Hong. Deep learning forecasting using time-varying parameters of the sird model for covid-19. *Scientific Reports*, 12(1):1–13, 2022.
- Fred Brauer, Carlos Castillo-Chavez, and Zhilan Feng. *Mathematical models in epidemiology*, volume 32. Springer, 2019.
- Centers for Disease Control and Prevention. Variants and genomic surveillance for sars-cov-2, 2022. URL <https://www.cdc.gov/coronavirus/2019-ncov/variants/variant-surveillance.html>. Accessed: 21-01-2022.
- Ian Cooper, Argha Mondal, and Chris G Antonopoulos. A sir model assumption for the spread of covid-19 in different communities. *Chaos, Solitons & Fractals*, 139:110057, 2020.
- Riccardo Delli Compagni, Zhao Cheng, Stefania Russo, and Thomas P Van Boeckel. A hybrid neural network-seir model for forecasting intensive care occupancy in switzerland during covid-19 epidemics. *PloS one*, 17(3):e0263789, 2022.
- The New York Times*. Coronavirus (covid-19) data in the united states. <https://github.com/nytimes/covid-19-data>, 2022. Accessed: 21-01-2022.
- Mevin B Hooten and Christopher K Wikle. A hierarchical bayesian non-linear spatio-temporal model for the spread of invasive species with application to the eurasian collared-dove. *Environmental and Ecological Statistics*, 15(1):59–70, 2008.
- Willem Hundsdorfer and Jan G Verwer. *Numerical solution of time-dependent advection-diffusion-reaction equations*, volume 33. Springer Science & Business Media, 2007.
- Wangping Jia, Ke Han, Yang Song, Wenzhe Cao, Shengshu Wang, Shanshan Yang, Jianwei Wang, Fuyin Kou, Penggang Tai, Jing Li, et al. Extended sir prediction of the epidemics trend of covid-19 in italy and compared with hunan, china. *Frontiers in medicine*, 7:169, 2020.
- Xinyi Lu, Perry J Williams, Mevin B Hooten, James A Powell, Jamie N Womble, and Michael R Bower. Nonlinear reaction–diffusion process models improve inference for population dynamics. *Environmetrics*, 31(3):e2604, 2020.
- R Core Team. *R: A Language and Environment for Statistical Computing*. R Foundation for Statistical Computing, Vienna, Austria, 2021. URL <https://www.R-project.org/>.
- Fabio Sigrist, Hans R Künsch, and Werner A Stahel. Stochastic partial differential equation based modelling of large space–time data sets. *Journal of the Royal Statistical Society: Series B (Statistical Methodology)*, 77(1):3–33, 2015.
- Gordon D Smith, Gordon D Smith, and Gordon Dennis Smith Smith. *Numerical solution of partial differential equations: finite difference methods*. Oxford university press, 1985.
- Stan Development Team. RStan: the R interface to Stan, 2022. URL <https://mc-stan.org/>. R package version 2.21.5.
- Gui-Quan Sun, Shi-Fu Wang, Ming-Tao Li, Li Li, Juan Zhang, Wei Zhang, Zhen Jin, and Guo-Lin Feng. Transmission dynamics of covid-19 in wuhan, china: effects of lockdown and medical resources. *Nonlinear Dynamics*, 101(3):1981–1993, 2020.
- US Census Bureau. Gazetteer Files, 10 2021. URL <https://www.census.gov/geographies/reference-files/time-series/geo/gazetteer-files.html>.
- Haiyan Wang and Nao Yamamoto. Using a partial differential equation with google mobility data to predict covid-19 in arizona. *arXiv preprint arXiv:2006.16928*, 2020.
- Christopher K Wikle. Hierarchical bayesian models for predicting the spread of ecological processes. *Ecology*, 84(6):1382–1394, 2003.
- Perry J Williams, Mevin B Hooten, George G Esslinger, Jamie N Womble, James L Bodkin, and Michael R Bower. The rise of an apex predator following deglaciation. *Diversity and Distributions*, 25(6):895–908, 2019.
- Nao Yamamoto, Bohan Jiang, and Haiyan Wang. Quantifying compliance with covid-19 mitigation policies in the us: A mathematical modeling study. *Infectious Disease Modelling*, 6:503–513, 2021.

Supplementary

1 Additional Descriptive Analysis

Figure 8 presents the daily cases with a 7-day moving average in the USA. There were three large spikes in the confirmed case numbers over the past two years. The first one occurred during the holiday season in 2020. Gatherings and celebrations accelerated the spread of the disease. In June 2021, the number of cases fell to the lowest point of the year. This decline was likely associated with the availability of vaccines. The second and third sharp increases were consistent with the emergence of delta and omicron variants. The data suggest that these variants are more transmissible than the original virus [Centers for Disease Control and Prevention, 2022]. Therefore, we can further modify the model by incorporating the key quantities as functions of potential covariates.

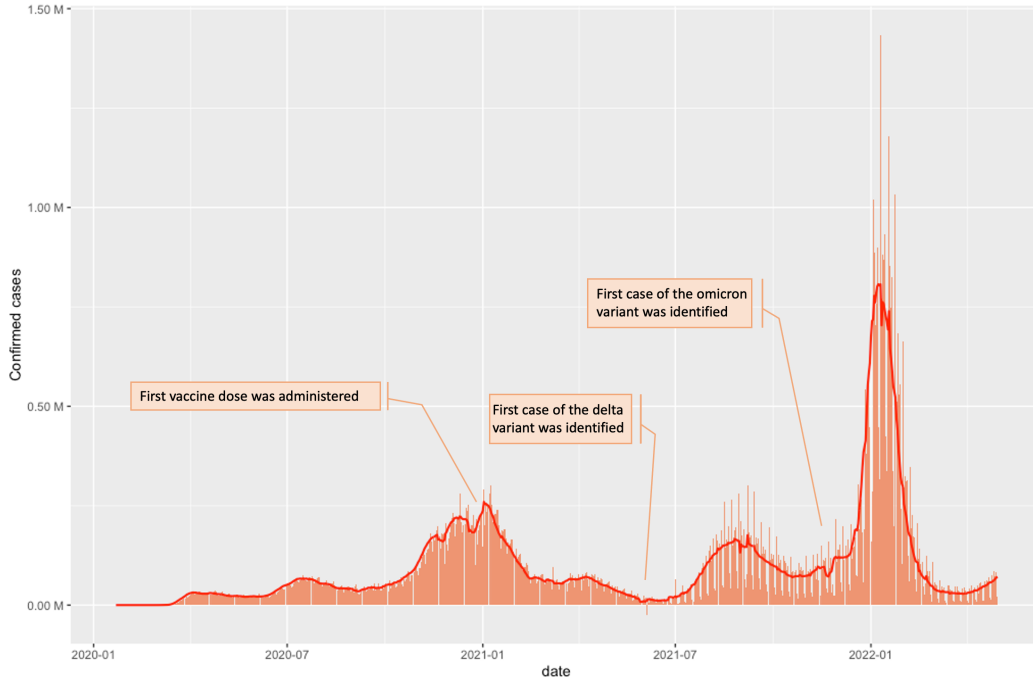


Figure 8: Daily Confirmed New Cases and 7-day Moving Average in the USA

2 Additional Simulation results

Figures 9 and 10 show the true values of the parameters and $\mathbf{u}(t; s)$ in simulation scenario 1, as well as their posterior means under Wikle's and proposed models. The proposed model 3 outperformed the others, with the closest estimation of parameters.



Figure 9: The True Values and the Posterior Means of Parameters from Different Models in Simulation Scenario 1

For the proposed model 3, we examine four different prior variances for advection, diffusion, and reaction rates. The estimated parameter values are presented in Figure 11. Based on the plot, it is evident that for variances less than or equal to 0.1, the parameters' estimates are close to their true values. The results indicate that the proposed model 3 is relatively robust. To resolve the problem of estimates deviating from the true values when the prior variances are large, we specify the correlations between random errors in the proposed model 5.

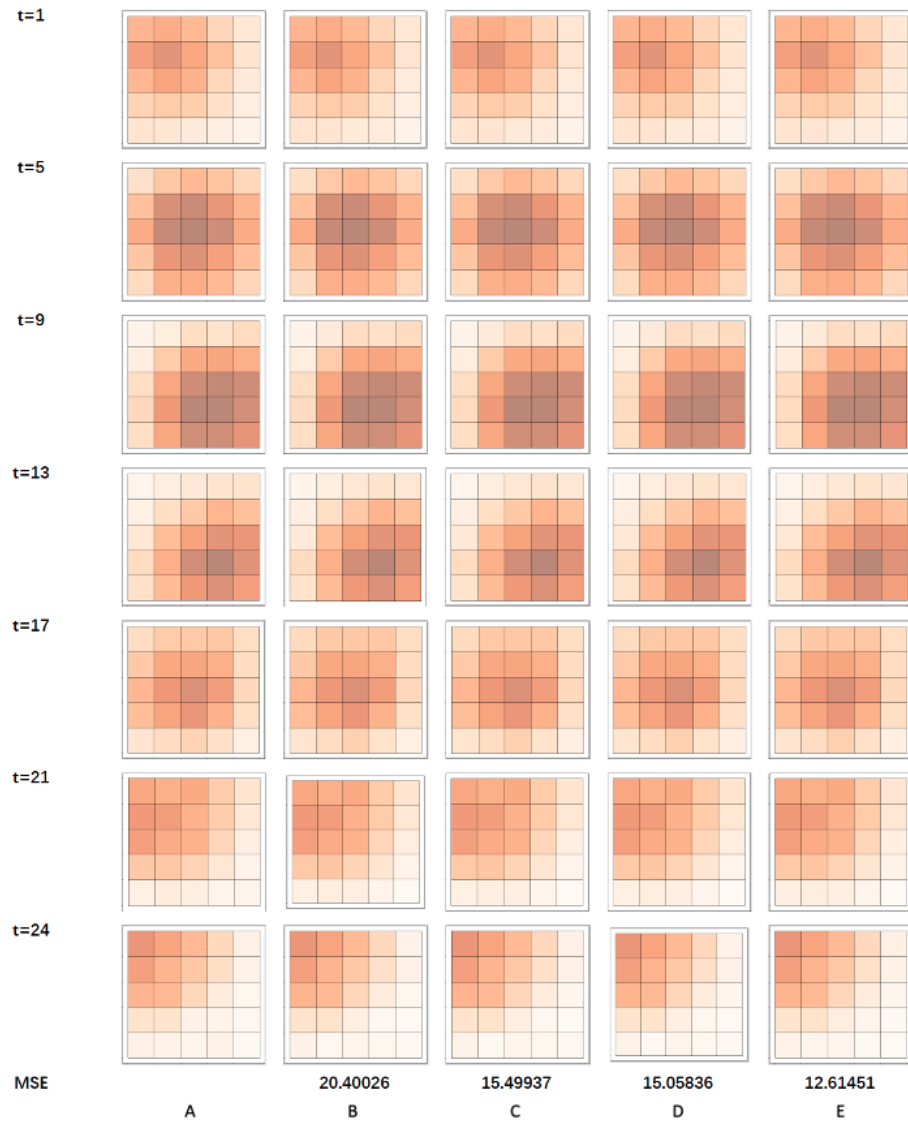


Figure 10: A. The True Values of \mathbf{u}_t ; the Estimated Values of \mathbf{u}_t with B. Wike's Model, C. Proposed Model 1, D. Proposed Model 2 and E. Proposed Model 3 in Simulation Scenario 1

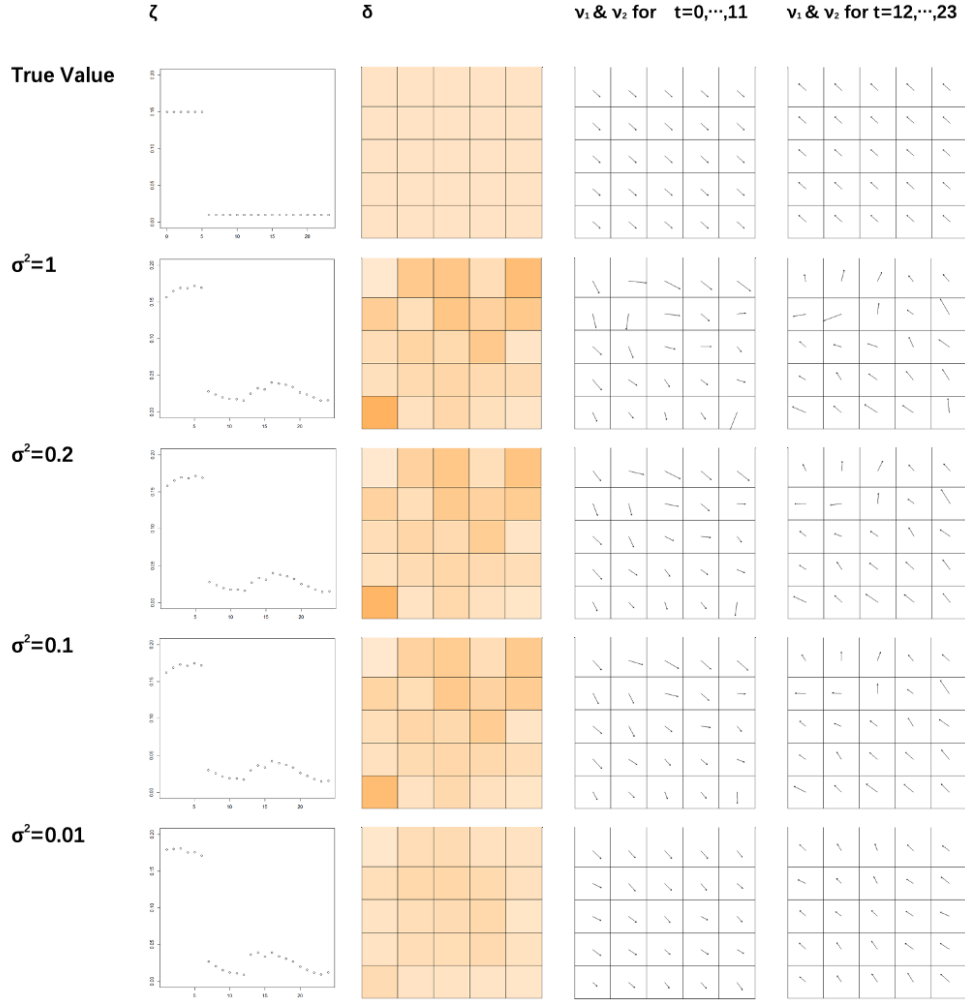


Figure 11: The True Values and the Posterior Means of Parameters with different prior distributions in Simulation Scenario 2